LBL-34559
UC-405
Preprint

Lawrence Berkeley Laboratory
UNIVERSITY OF CALIFORNIA

Physics Division

Mathematics Department

Submitted for publication

Numerical Computation of Self-Similar Solutions for Mean Curvature Flow

D.L. Chopp

August 1993

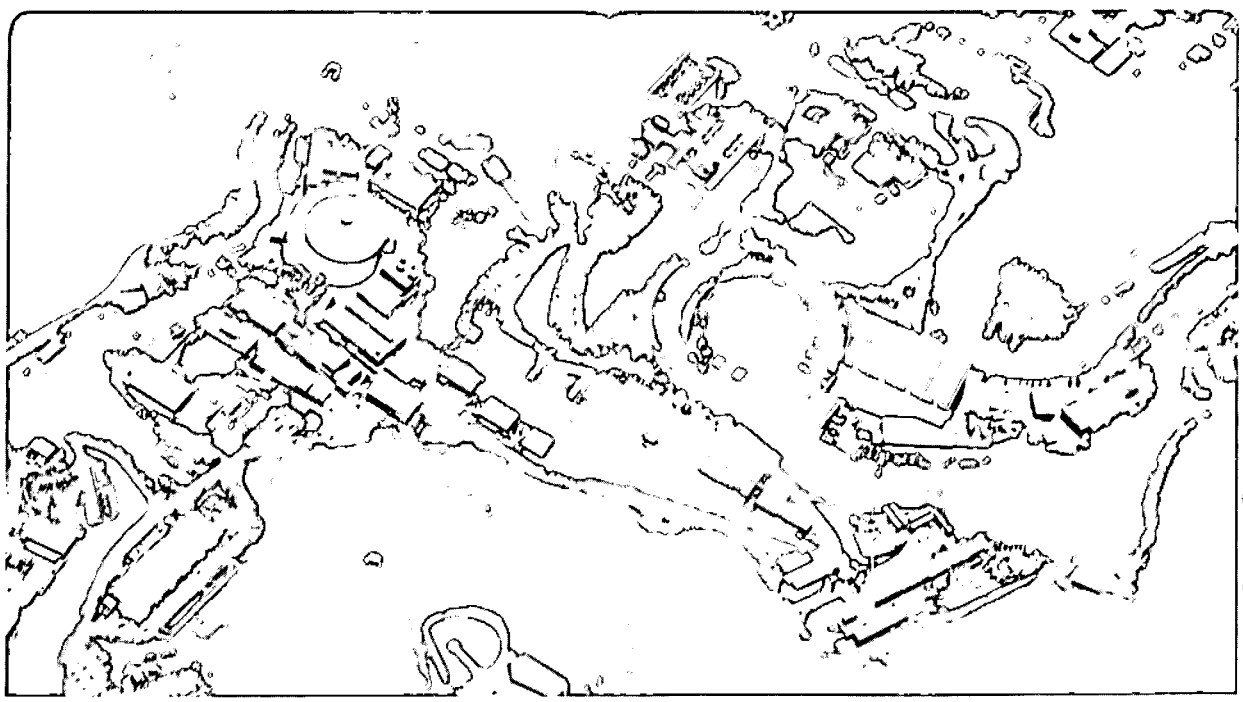

REFERENCE COPY
Does Not
Circulate
Bldg. 50 Library.
LBL-34559
Copy 1

Prepared for the U.S. Department of Energy under Contract Number DE-AC03-76SF00098

DISCLAIMER

This document was prepared as an account of work sponsored by the United States Government. While this document is believed to contain correct information, neither the United States Government nor any agency thereof, nor the Regents of the University of California, nor any of their employees, makes any warranty, express or implied, or assumes any legal responsibility for the accuracy, completeness, or usefulness of any information, apparatus, product, or process disclosed, or represents that its use would not infringe privately owned rights. Reference herein to any specific commercial product, process, or service by its trade name, trademark, manufacturer, or otherwise, does not necessarily constitute or imply its endorsement, recommendation, or favoring by the United States Government or any agency thereof, or the Regents of the University of California. The views and opinions of authors expressed herein do not necessarily state or reflect those of the United States Government or any agency thereof or the Regents of the University of California.

LBL-34559

NUMERICAL COMPUTATION OF SELF-SIMILAR SOLUTIONS FOR MEAN CURVATURE FLOW[1]

David L. Chopp

Lawrence Berkeley Laboratory
University of California
Berkeley, CA 94720

August 1993

[1] This work was supported in part by a National Science Foundation Fellowship, by the Office of Naval Research under Contract N0001493WX22029, by DARPA/AFOSR under Contract F-49620-87-C-0065, and by the Applied Mathematical Sciences Subprogram of the Office of Energy Research, U.S. Department of Energy under Contract DE-AC03-76SF00098.

Numerical Computation of Self-Similar Solutions for Mean Curvature Flow

David L. Chopp*
Lawrence Berkeley Laboratory
University of California
Berkeley, CA 94720

August 31, 1993

1 Introduction

Self-similar solutions of motion by mean curvature are an important component in the current research of the singularities in that motion. There appears to be a link between singularities in motion by mean curvature and self-similar shapes. For curves in R^2, Grayson [12] has proven that curves under motion by curvature shrink to round points. Alternatively, this shows that every closed embedded curve in R^2 deforms towards a self-similar solution as it approaches singularity, and that a circle is the only such self-similar solution. Therefore, Grayson's result effectively shows the connection between self-similar solutions and singularity.

For two-dimensional manifolds in R^3, the problem is much more difficult and not as well understood. However, two results by Huisken indicate that self-similar solutions and singularities are connected in this higher dimension as well. The first result, see [14], shows that convex manifolds shrink to spheres under motion by mean curvature. In [13], Grayson was able to prove that the convexity condition is necessary. In a recent paper by Angenent [2], he first proves the existence of a self-similar torus, then uses that torus to give an alternative proof that the convexity condition is necessary. This demonstrates the utility of self-similar solutions towards studying singularities. The best result showing the link between self-similarity and singularity is by Huisken [15] where he proves that if the curvature at a singularity is bounded by $c(T-t)^{-1/2}$, where t is time,

*This work was supported in part by a National Science Foundation Fellowship, by the Office of Naval Research under contract N0001493WX22029, by DARPA/AFOSR under contract No. F-49620-87-C-0065, and by the Applied Mathematical Sciences Subprogram of the Office of Energy Research, U.S. Department of Energy under contract DE-AC03-76SF00098.

T is the time of singularity and c is a constant, then the surface evolves towards a self-similar surface at the point of singularity.

A second theoretical question involving self-similar surfaces for mean curvature flow involves the weak solution for mean curvature flow. It is known for 1-dimensional curves that self-intersect, the weak solution for curvature flow dictates that the curve develops a nonempty interior because of the point of self-intersection. However, Grayson's result shows that a smooth curve will not self-intersect, and hence not develop an interior.

We may ask the same question about higher dimensional surfaces flowing by mean curvature. Notice that a torus which initially has a large ratio m_2/m_1 (see Figure 2) develops a singularity in the center of the hole as it evolves towards a sphere. On the other hand, a torus with small ratio m_2/m_1 evolves towards a circle as the cross-sectional area goes to zero. It was once conjectured that a torus with an initial ratio on the boundary of these two regimes would develop an interior. However, the discoveries by Angenent and Huisken have shown that instead, this particular torus evolves into a self-similar torus. The question of whether arbitrary smooth initial surfaces can develop an interior remains open, but we believe the "Double Handle" example presented below may prove to be an example of this phenomenon for two-dimensional surfaces.

In related work, some progress on the occurence of singularities and evolution past singularities for surfaces of revolution has been made in a recent paper by Altshuler, Angenent and Giga [1].

At present, very few examples of two-dimensional embedded self-similar solutions for motion by mean curvature are proven to exist, all of them being surfaces of revolution. In this paper, we design a numerical algorithm to compute approximations to other self-similar solutions. We will give strong numerical evidence that these are good approximations to self-similar solutions.

In the next section we describe the algorithm including the modified form of motion by mean curvature differential equation. In the following section, we discuss the reliability of the results in several different ways. In the final section we show a collection of approximate self-similar solutions for motion by mean curvature.

2 The Algorithm

2.1 Overview

The algorithm we use is based upon the level set method for propagating interfaces introduced by Osher and Sethian [16]. The numerical methods which led up to the level set method can be found in [17], and for a review of numerical methods for curvature flow see [18]. The theoretical aspects of this method were studied by Evans and Spruck [8, 9]. For further theoretical work, see also [3, 7, 10, 11]. The level set method has been applied to a number of other

applications, for example, see [5, 4, 6, 19].

It will be helpful to give a brief overview of the level set method as it applies here. The idea behind the level set method is to represent a given two-dimensional manifold as a level set of a function $\phi : R^3 \times R \to R$. Thus, the set

$$S_\alpha(t) = \{x \in R^3 : \phi(x,t) = \alpha\}$$

represents the evolution of the α-level set in time t. Motion by mean curvature can now be expressed in terms of ϕ by

$$\phi_t(x,t) = H_\phi(x,t)||\nabla\phi(x,t)||$$

where $H_\phi(x,t)$ is the mean curvature of the $\phi(x,t)$ level set. Notice that this equation does not depend upon the level set value, each level set surface moves according to its own mean curvature. In this way, this equation evolves a continuous family of initial surfaces by mean curvature simultaneously. It is this property which is at the heart of our algorithm.

2.2 An Example: The Self-Similar Torus

We introduce the self-similar algorithm by studying the case of finding a self-similar torus. let $\mathcal{M}$ be the space of all compact two-dimensional differentiable manifolds embedded in R^3. For any two manifolds A, $B \in \mathcal{M}$, define the equivalence relation $A \sim B$ if B can be obtained from A by rigid body motion, rotation, and uniform stretching. Now let $M = \mathcal{M}/\sim$.

Let $C = \{x = (x_1, x_2, x_3) \in R^3 : x_1^2 + x_2^2 = 1, x_3 = 0\}$ and define $S_\lambda(0) = \{x \in R^3 : \text{dist}(x, C) = \lambda\}$. Thus, $S_\lambda(0)$ is a one-dimensional subspace of M parameterized by $\lambda \in (0,1)$. For each λ, let $S_\lambda(t)$ be the result of moving $S_\lambda(0)$ by mean curvature to time t, and define T_λ as the time to singularity for the initial surface $S_\lambda(0)$. We now have a subset $U = \{S_\lambda(t) : \lambda \in (0,1), t \in [0, T_\lambda)\} \subset M$. A diagram of U is shown in Figure 1.

Next, we define a ratio function $\rho : U \to R$, $\rho(A) = m_2/m_1$, where m_2 is the maximum height of the torus in the z direction and m_1 is the innermost radius of the torus as shown in Figure 2. Thus, $\rho(S_\lambda(0)) \to +\infty$ as $\lambda \to 1^-$ and $\rho(S_\lambda(0)) \to 0^+$ as $\lambda \to 0^+$. We rescale U in terms of ρ and t so that U is contained in the shaded region in Figure 3.

If we turn our attention now to the trajectories $S_\lambda(t)$, $t \in [0, T_\lambda)$, we see that there is a value λ_0 such that if $\lambda > \lambda_0$, then $\rho(S_\lambda(t)) \to +\infty$, $\frac{d}{dt}\rho(S_\lambda(t)) > 0$, as $t \to T_\lambda$ and if $\lambda < \lambda_0$, then $\rho(S_\lambda(t)) \to 0$, $\frac{d}{dt}\rho(S_\lambda(t)) < 0$. Using the fact we have continuous initial data, we hope that for $\lambda = \lambda_0$, $\frac{d}{dt}\rho(S_{\lambda_0}(t)) \to 0$ as $t \to T_{\lambda_0}$ and $\rho(S_{\lambda_0}(t)) \to \rho_0$ for some finite constant $\rho_0 > 0$. Thus, our picture of U including trajectories should look like Figure 4. We computed these trajectories for a small number of initial surfaces $S_\lambda(0)$ for λ near λ_0. The results are given by the solid lines in Figure 5. Our goal then, is to locate the special trajectory $S_{\lambda_0}(t)$.

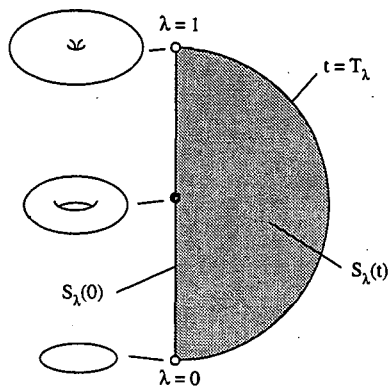

Figure 1: Diagram of $U \subset M$

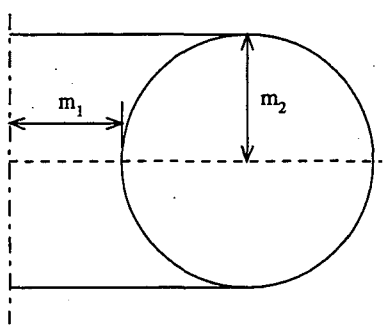

Figure 2: Measurements of a torus for computing ρ.

In general, we cannot a priori compute λ_0 exactly. Regardless of how small $|\lambda - \lambda_0| > 0$ is, $S_\lambda(t) \not\to S_{\lambda_0}(t)$ as $t \to T_\lambda$. In fact, $S_\lambda(t)$ does not even provide a good approximation because of the instability of the problem. Figure 5 shows how quickly $S_\lambda(t)$ (the solid lines) diverge, even those starting very close to $S_{\lambda_0}(t)$ at $t = 0$.

Therefore, we must find some other means of locating the trajectory $S_{\lambda_0}(t)$. To do this, we first define $R(\lambda, t) = \rho(S_\lambda(t))$. For $\lambda < \lambda_0$, $R(\lambda, t) \to 0$, $\frac{\partial R}{\partial t}(\lambda, t) < 0$ as $t \to T_\lambda$. Similarly, for $\lambda > \lambda_0$, $R(\lambda, t) \to +\infty$, $\frac{\partial R}{\partial t}(\lambda, t) > 0$ as $t \to T_\lambda$. Also, if the curvature does not blow up too fast, then we may conclude $\frac{\partial R}{\partial t}(\lambda_0, t) \to 0$ as $t \to T_{\lambda_0}$. Thus, we define $\tilde{\lambda}_0(t)$ such that $\frac{\partial R}{\partial t}(\tilde{\lambda}_0(t), t) \equiv 0$. The dashed line in Figure 5 depicts the function $R(\tilde{\lambda}_0(t), t)$. Then the idea of the algorithm for finding a self-similar solution is to compute $\lim_{t \to T_{\lambda_0}} S_{\tilde{\lambda}_0(t)}(t)$.

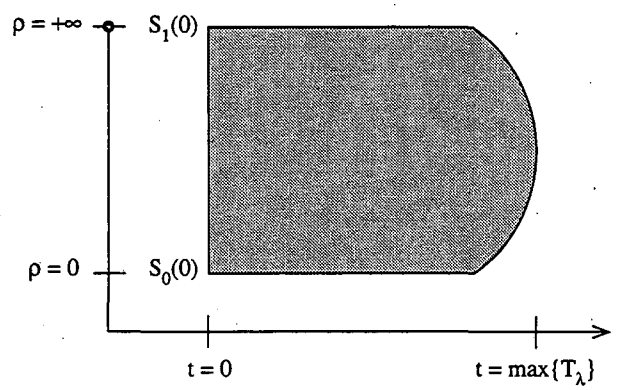

Figure 3: Rescaled diagram of U.

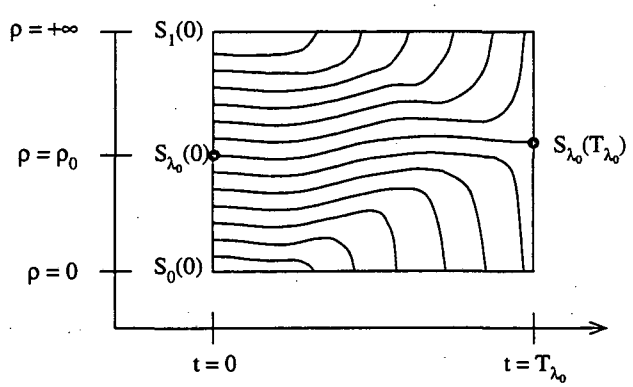

Figure 4: Plot of trajectories for $S_\lambda(t)$

2.3 The General Algorithm

We now give the details of the general method. Recall that the level set formulation for curvature flow can be expressed as

$$\phi_t = H_\phi ||\nabla \phi||. \tag{1}$$

We define a new function ψ as

$$\psi(x,t) = \phi(\sigma(t)x,t)/\sigma^2(t) - L(t). \tag{2}$$

Differentiating Equation 2 with respect to t and combining with Equation 1 produces a new partial differential equation for ψ given by

$$\psi_t = \frac{\sigma'(t)}{\sigma(t)}(x \cdot \nabla\psi - 2(\psi + L(t)) + H_\psi ||\nabla\psi|| - L'(t). \tag{3}$$

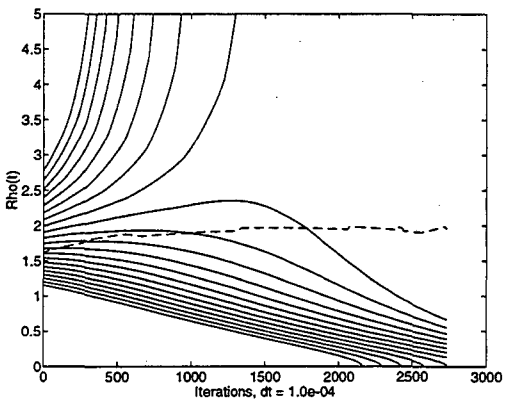

Figure 5: Computed trajectories of $S_\lambda(t)$

Here H_ψ is the mean curvature of the level set surface of ψ through the point (x,t).

The functions $\sigma(t)$ and $L(t)$ are determined dynamically as time evolves. The stretching function $\sigma(t)$ is chosen so that the zero level set of ψ has constant volume for all t. Let $V(t) = \text{Volume}(\psi(\cdot,t)^{-1}(0))$, then

$$\sigma(t) = \left(\frac{V(t)}{V(0)}\right)^{1/3}$$

so that

$$\frac{\sigma'(t)}{\sigma(t)} = \frac{V'(t)}{3V(t)}.$$

The level function $L(t)$ is given by the equation

$$\frac{\partial R}{\partial t}(L(t),t) = 0.$$

In this context, we have $S_{\tilde{\lambda}_0(t)}(t) = \psi^{-1}(\cdot,t)(0)$.

We compute $\psi(x,t)$ numerically in a three step explicit scheme. The three steps are summarized below where $\psi_n \equiv \psi(x_{ij},t_n)$, $\Delta t = t_{n+1} - t_n$.

1. $\tilde{\psi}_{n+1} = \psi_n + ||\nabla\psi_n||H(\psi_n)\Delta t.$
2. (a)
   - $V_{n+1} = \text{Volume}(\tilde{\psi}_{n+1}^{-1}(0))$
   - $V_n = \text{Volume}(\psi_n^{-1}(0))$

   (b)
   - $R_n(\ell) = \rho(\psi_n^{-1}(\ell))$
   - $R_{n+1}(\ell) = \rho(\tilde{\psi}_{n+1}^{-1}(\ell))$

- $L_{n+1} = (R_{n+1}(\cdot) - R_n(\cdot))^{-1}(0)$

3. $\psi_{n+1} = \tilde{\psi}_{n+1} + \frac{V_{n+1}-V_n}{3V_n}(x \cdot \nabla\psi_n - 2(\psi_n + L_n)) - (L_{n+1} - L_n)$

The first step is identical to the standard explicit numerical implementation of Equation 1. This is where the curvature flow terms appear. The second step is where $\sigma(t)$ and $L(t)$ are determined according to information obtained from the curvature flow in the first step. The third step makes the corrections to ψ needed due to the stretching and level set shifting predicted by the second step. Note that combining the first and third steps results in a straightforward explicit discretization of Equation 3.

In all cases, central differencing was used for spatial derivatives except for the term $x \cdot \nabla\psi_n$ where upwind differencing was used,

$$\begin{aligned} x \cdot \nabla\psi_n &= \max(0,x)D^x_-\psi_n + + \max(0,y)D^y_-\psi_n + \max(0,z)D^z_-\psi_n \\ &\quad + \min(0,x)D^x_+\psi_n + \min(0,y)D^y_+\psi_n + \min(0,z)D^z_+\psi_n. \end{aligned}$$

This follows the discretization used in [16].

2.4 Notes About the Algorithm

2.4.1 Delay of Level Switching

Recall that $\frac{\partial R}{\partial t}(\lambda_0, t) \to 0$ as $t \to T_{\lambda_0}$, however this is expected only in a neighborhood of T_{λ_0}. In practice, $\left|\lambda_0 - \frac{\partial R}{\partial t}(\cdot, 0)^{-1}(0)\right|$ can be large causing problems numerically for small t. For that reason, we make a preliminary estimate of λ_0 by $\tilde{\lambda}_0$ using a bisection method, then step 2(b) for updating $L(t)$ is changed to

2. (b) $\ell = (R_{n+1}(\cdot) - R_n(\cdot))^{-1}(0)$
   If $|L_n - \ell| < \epsilon$ then $L_{n+1} = \ell$ else $L_{n+1} = \tilde{\lambda}_0$.

This amendment delays the traversing of level sets until t is in a neighborhood of T_{λ_0}. We can see why this is a necessary precaution for small t in Figure 5 where $R(\tilde{\lambda}_0(t), t)$ (the dashed line) is not near the best approximation to $R(\lambda_0, t)$ (the middle solid line) for small t.

2.4.2 Time Scale and Reinitialization

It is worth noting that the equation of motion used here differs from the equations used by Huisken and others. In our equations we have not used rescaling in time to prevent singularity in finite time. We have done this for two reasons, first, we do not have a means of accurately computing the time of singularity for a given surface, and second, we must complete the computation in finite time.

This also means that at the time of singularity, the computation must go unstable. This means that we cannot compute all the way up to time T, but must stop short. We find that smaller grid sizes are capable of remaining stable

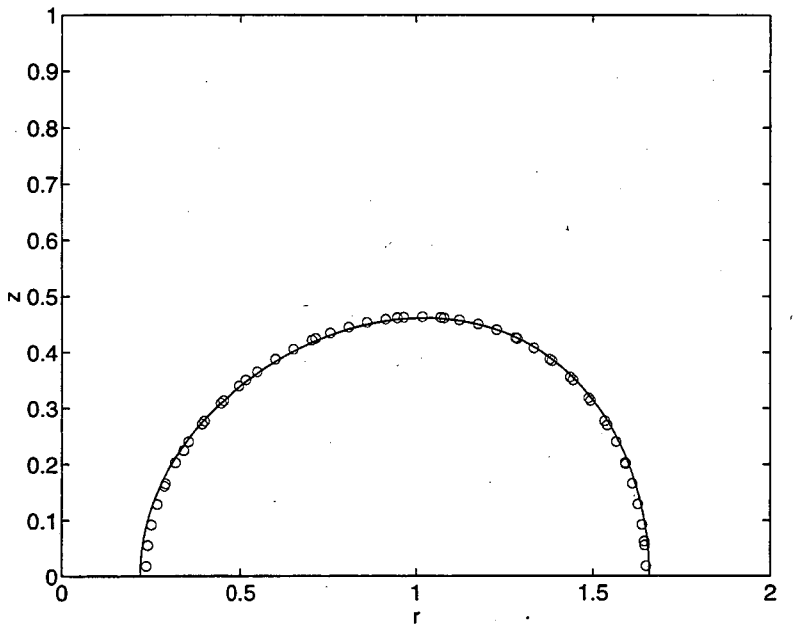

Figure 6: Comparison of computed and exact torus solutions

longer than courser grid sizes, but the length of stability is also dependent upon the surface we are computing.

To compensate for this shortcoming, we periodically use reinitialization of the level set function ψ. When the calculation is approaching the time of singularity, we stop the computation and restart using the current zero level set Z as the initial surface. The function ψ is then computed using the signed distance function from Z. The gain from reinitialization decreases rapidly with each use, so a typical computation will use as few as one reinitialization and no more than ten.

3 Tests for Self-Similarity

In Figure 6, we compare the profiles of the exact solution of the self-similar torus solution as derived from [2] represented by the solid line with the computed solution using our algorithm represented by the circles. The graph shows we have good agreement between these two solutions. For the other cases where an exact solution is not known, we will use other tests for self-similarity. For each test we will use the error for the computed torus solution as a benchmark for

other solutions.

The first test of self-similarity is based upon a simple condition which is easily shown to be sufficient for self-similarity. We follow the argument presented by Huisken in [15]. Suppose that Γ_0 is a 2-manifold such that for each point $x \in \Gamma_0$,

$$H(x) = (2T)^{-1/2} x \cdot n \tag{4}$$

where n is the unit normal to Γ_0 at x, and T is some constant. Define $\Gamma_t = (2(T-t))^{1/2}\Gamma_0$. Then

$$\left(\frac{d}{dt}\Gamma_t\right)^{\perp} = \frac{-1}{(2(T-t))^{1/2}} H_0 \cdot n = -Hn. \tag{5}$$

Therefore, Γ_t is equivalent to curvature flow with initial surface Γ_0 and hence Γ_0 must be a self-similar solution. The constant T is the time to singularity for the surface Γ_0.

Given a surface S, we implement Equation 4 numerically by sampling evenly on S to get values x_i, n_i, and H_i for $i = 1,\ldots,N$. The constant $C = \sqrt{2T}$ is estimated by

$$C \approx \tilde{C} = \frac{\sum_{i=1}^{N} x_i \cdot n_i}{\sum_{i=1}^{N} H_i}.$$

The computed error estimate is given by

$$E = \frac{1}{N}\sqrt{\sum_{i=1}^{N}\left(H_i - \frac{1}{\tilde{C}} x_i \cdot n_i\right)^2}.$$

For the computed torus on a rectangular grid of dimensions $90 \times 90 \times 90$ with space step size $\Delta x = 2.24 \times 10^{-2}$, the computed error is $E = 0.034354$. We conclude a surface is near self-similarity if E is of the same order as the computed error for the torus.

The second test is related to the first, but allows for differences in scale. If we plot the data points computed on a given surface with $\frac{1}{\tilde{C}} x_i \cdot n_i$ versus H_i, then the points should fill a diagonal line segment. We show the plot for the computed torus solution. Surfaces that fail this test tend to show some structure forming a significant angle to the expected line segment and do not decrease with time or grid refinement.

Finally, for compact surfaces, we start with the computed solution and evolve it according to normal mean curvature flow. A self-similar solution should retain its shape for a considerable time as it shrinks.

4 Computed Solutions

For each of the examples of computed solutions given below, we will describe the initial level sets and the measurements used for the ratio function $R(\lambda, t)$.

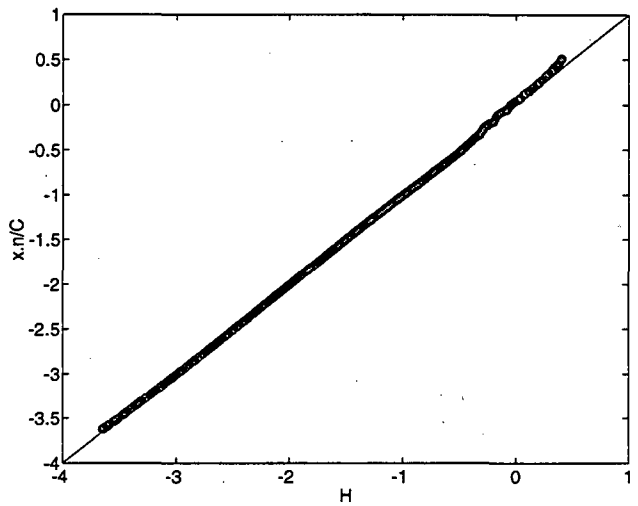

Figure 7: Graph of $\frac{1}{C}x_i \cdot n_i$ versus H_i for torus

We will follow that with pictures of the surface along with results from the tests discussed from the previous section and a brief summary.

4.1 The "Cube"

We begin with a genus 5 surface we call the "cube". The initial surface consisted of a sphere minus cylinders along the coordinate axes as depicted in Figure 8. The other level sets were equidistant contours from that initial surface. The ratio function measured the distance from the origin to the furthest point of the surface in the direction of the vector $(1, 1, 1)$ over the minimum radius of the hole along the x-axis as shown in Figure 9.

The evolution of the surface by this method is shown in Figure 10. The initial figure is a sphere minus cylinders. For the first portion of the evolution, the level set switching is turned off and hence the initial surface evolves towards a surface where the holes would expand and break the connecting arms. However, after the level set switching is activated, the holes begin shrinking again and the surface converges towards the final solution.

The final computed solution is shown in Figure 11. The computation was performed on a $60 \times 60 \times 60$ grid with space step $\Delta x = 3.39 \times 10^{-2}$. The computed error for this surface is $E = 2.886 \times 10^{-2}$. The plot of $\frac{1}{C}(x_i \cdot n_i)$ versus H_i is shown in Figure 12. This plot shows the characteristic lining up along the diagonal of the points on the surface. Finally, we show in Figure 13 one octant of this surface next to the same surface after it has evolved during

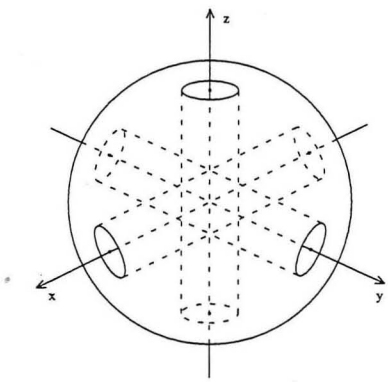

Figure 8: Initial surface for cube

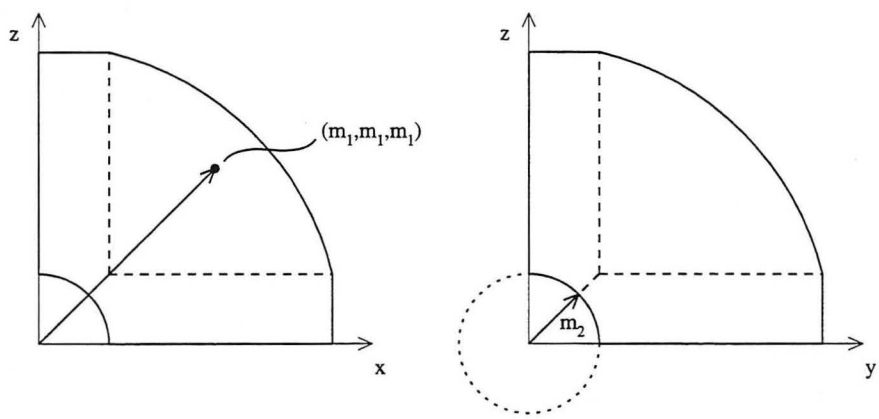

Figure 9: Ratio measurements for cube

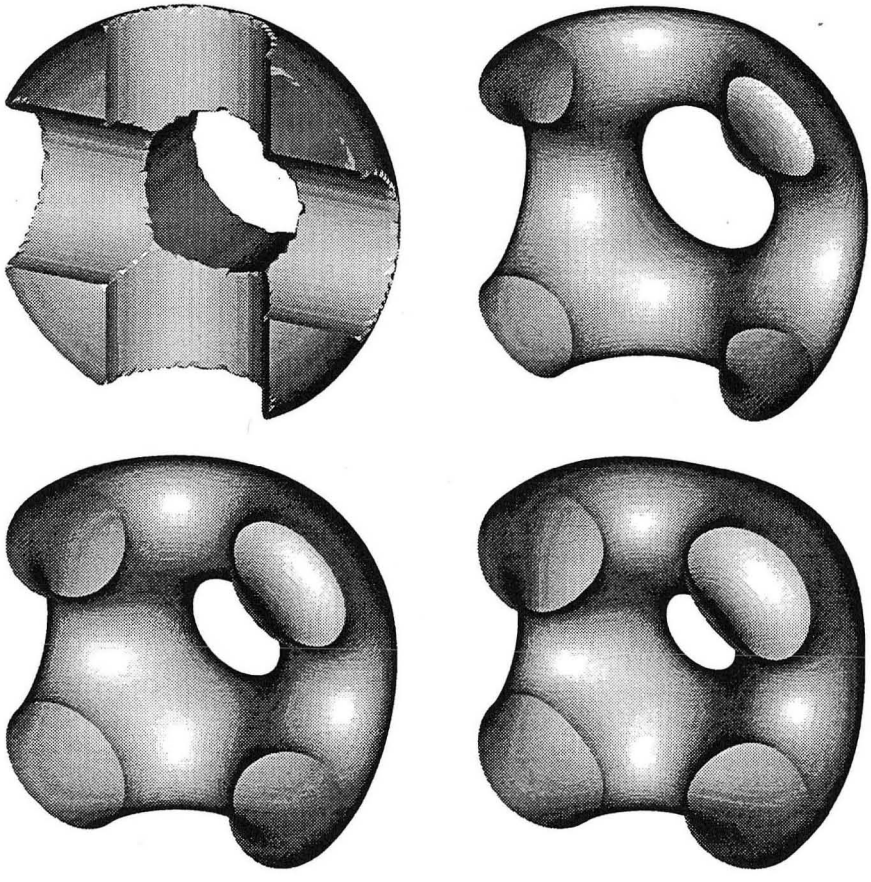

Figure 10: Evolution of cube surface

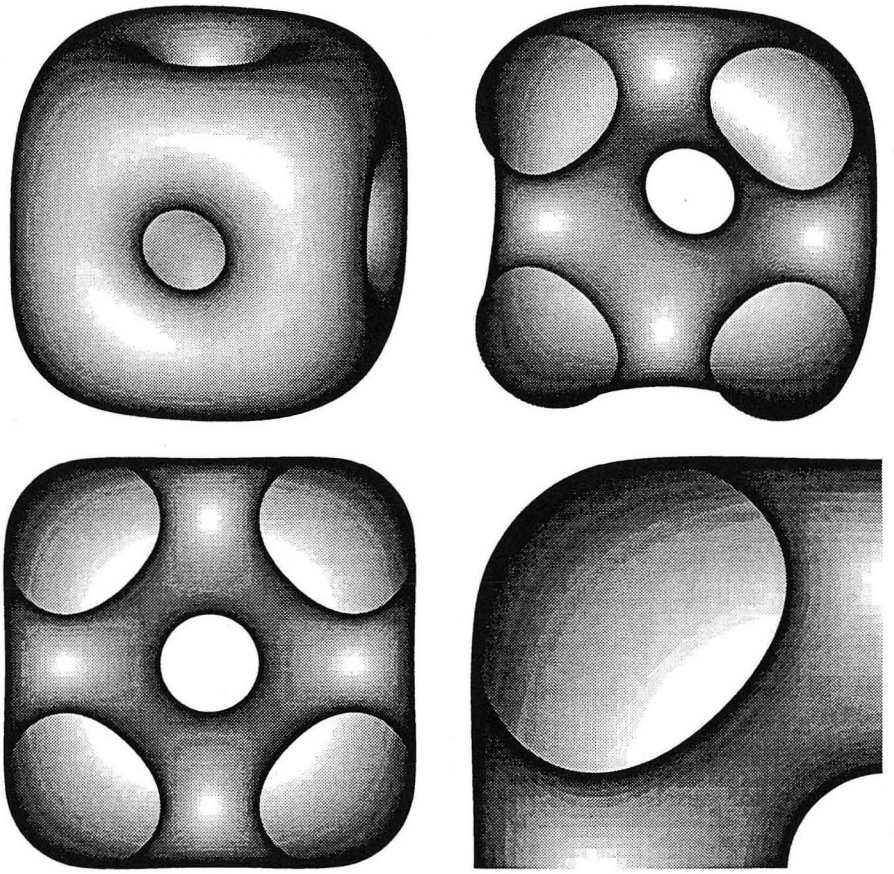

Figure 11: Pictures of the cube self-similar solution

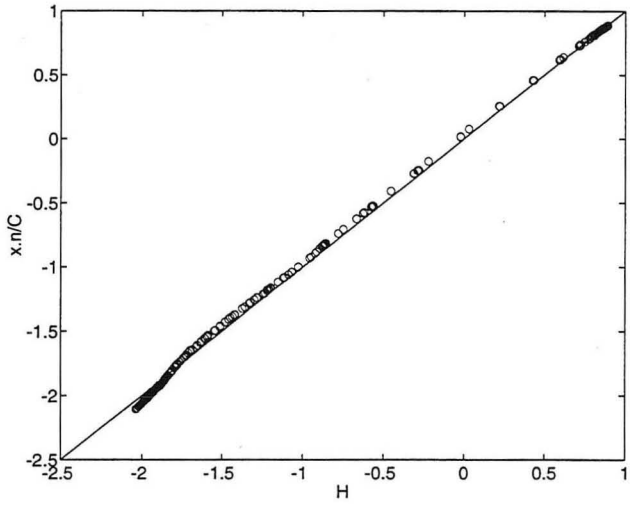

Figure 12: Graph of $\frac{1}{C}x_i \cdot n_i$ versus H_i for cube

normal mean curvature flow. Notice that it has retained its shape very well despite shrinking to almost 1/8 of its original volume.

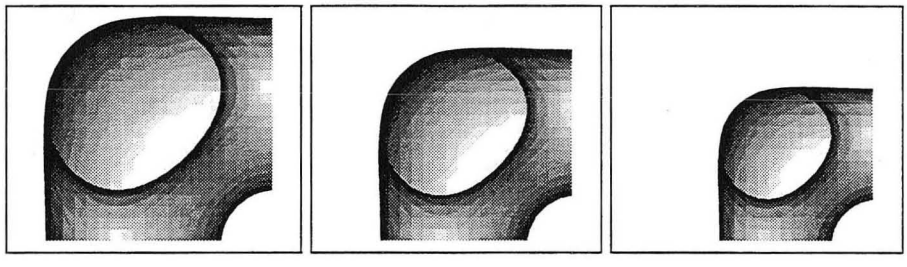

Figure 13: Cube surface evolved by mean curvature flow

The cube surface appears to pass all the tests for self-similarity within the guidelines of the computed torus solution, so we expect that this surface is a good approximation to a self-similar solution. This surface leads to the conjecture that every regular polyhedron with holes will produce a corresponding self-similar solution for mean curvature flow.

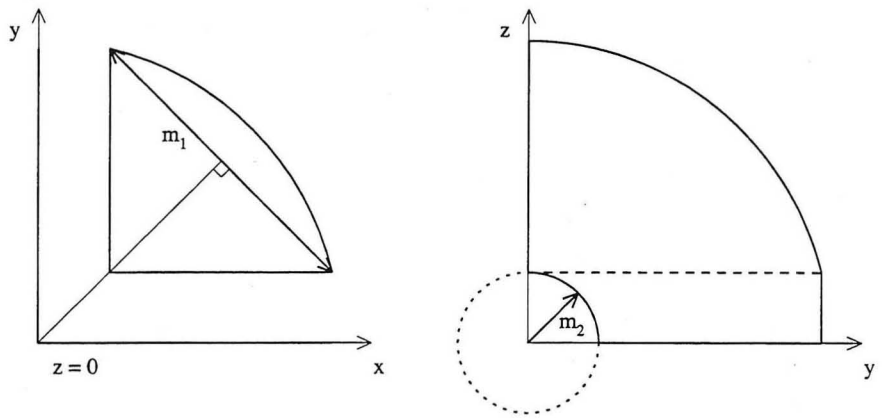

Figure 14: Ratio function measurements for the cube without one hole

4.2 The "Cube Minus One Hole"

A natural next attempt for the algorithm would be to try other symmetric arrangements of holes through a sphere. For example, we started with an initial surface as described for the cube, except the hole along the z-axis is removed. Again, the other initial level sets are equidistant contours from this surface. We tried a few different ratio function measurements all with the same end results. One such pair of measurements consists of measuring the minimum width of the hole along the x-axis against the maximum width of one of the four holes made by the surface sliced by the xy-plane. We show these measurements in Figure 14

The final computed solution was underresolved in the center for every grid size we used. The best resolution produced the surface shown in Figure 15. The grid size for this surface is $60 \times 60 \times 120$ with space step $\Delta x = 3.39 \times 10^{-2}$. The computed error for this surface is $E = 5.14 \times 10^{-1}$ and the plot of $\frac{1}{C}(x_i \cdot n_i)$ versus H_i is in Figure 16.

Notice in Figure 16 the additional branch of points. This tail does not diminish with time as for other surfaces. The computed error is also much larger than acceptable to conclude this surface is self-similar. We consider a number of possibilities about why this surface failed to evolve towards self-similarity.

First, the size of the two spheres is so much larger than the central structure that we were unable to adequately resolve both. We would hope that if there is a finite size for the spheres for which a self-similar solution exists, that increasing the number of grid points along the central axis would eventually lead to a resolution of both structures. We were unable to generate enough points to resolve this issue.

Second, there is no self-similar solution with this geometric configuration. In

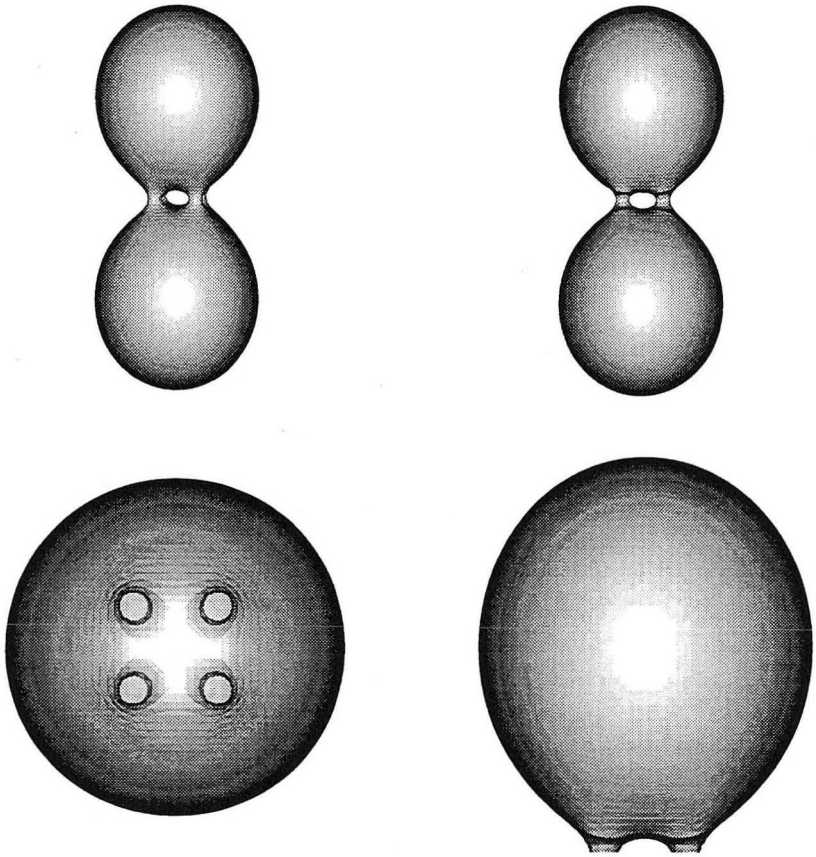

Figure 15: Computed solution for the cube minus one hole

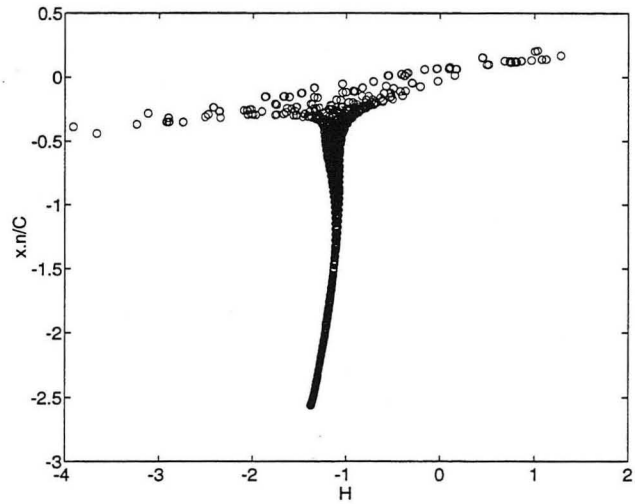

Figure 16: Graph of $\frac{1}{C}x_i \cdot n_i$ versus H_i for cube minus one hole

this category, we would consider the case where the spheres of the previous case actually grow indefinitely. In this case, we consider that the surface may not be compact, similar to the "Double Handle" surface presented below. We also considered the case where a compact solution exists, but where instead we start with an initial surface which looks like a symmetric 4-handle body. In light of the "Double Handle" surface results, we believe that this is the best conclusion.

Third, we are close to a candidate for a surface that develops an interior. As discussed in the introduction, the question of whether a smooth 2-dimensional surface can develop an interior remains an open question. If a bifurcation of initial surfaces exists for which the central one develops an interior as the conjecture suggests, then this algorithm must fail to find a self-similar solution for that case. It is amongst the failures of this algorithm that such a special bifurcation may exist.

The first and third possibilities are now beyond the scope of our algorithm, and we are still exploring the second. In any case, this particular configuration failed to produce a self-similar solution.

4.3 The "Octohedron"

In view of the this result, we return to the first conjecture that any regular polyhedron with holes drilled through the faces to the center will produce a self-similar solution and attempt to find a solution based upon a regular octahedron. Again we begin with a sphere, this time with holes drilled diagonally along the

vectors $(\pm 1, \pm 1, \pm 1)$. The remainder of the construction follows the construction for the cube. The surface this time has genus 7.

The final solution for the octahedron is shown in Figure 17. The computation was on a $80 \times 80 \times 80$ grid with $\Delta x = 2.53 \times 10^{-2}$. The computed error for this surface is $E = 3.33 \times 10^{-2}$ and the error plot is shown in Figure 18. In Figure 19, we show the the initial solution and the result of evolving the surface. For this surface, we get results which are sufficient to believe that the octahedron surface is a self-similar solution.

4.4 The "Punctured Saddle"

The next solution we show is a genus 2 solution suggested by Matt Grayson and Tom Ilmanen. The initial surface consists of the xy-plane combined with two crossing tubes at the origin as shown in Figure 20. The remaining level sets were equidistant contours from the initial surface. The nature of the symmetry of this surface made it unnecessary to use a ratio function. We expect the zero level set to always be the correct level set to find a self-similar solution of this form.

Another difference from the presented algorithm is in the computed volume. In this example, the volume on either side is exactly the same regardless of how thin the handle gets. For that reason, we used the cross-sectional area of one handle raised to the power 3/2 in order to simulate a constant volume property.

The original surface is assumed to be unbounded, the boundary conditions at the edges of the computational domain were taken to be upwind. This presented no problems as the stretching function ensured that the upwind direction is always in the direction of the origin.

In Figure 21, we show how the evolution proceeds. The two handles in the center expand outward and the holes in the plane tilt back to form the final surface.

The final computed solution is shown in Figure 22. The computation was performed on a 100x100x100 grid with space step $\Delta x = 2.02 \times 10^{-2}$. The computed error for this surface is $E = 2.005 \times 10^{-2}$. The plot of $\frac{x_i \cdot n_i}{2T}$ versus H_i is shown in Figure 23. For purposes of computing the error, the points of the surface on the boundary of the domain have been excluded.

The tests for self-similarity indicate that this surface is indeed self-similar. However, those tests could only be applied to that portion contained in the domain. Whether there exists an entire surface which is self-similar cannot be demonstrated with this algorithm.

4.5 The "Double Handle"

The last solution we show is a genus 3 solution inspired by the success of the "Punctured Saddle". The initial surface consists of two planes parallel to the xy-plane combined with three crossing tubes as shown in Figure 24. The

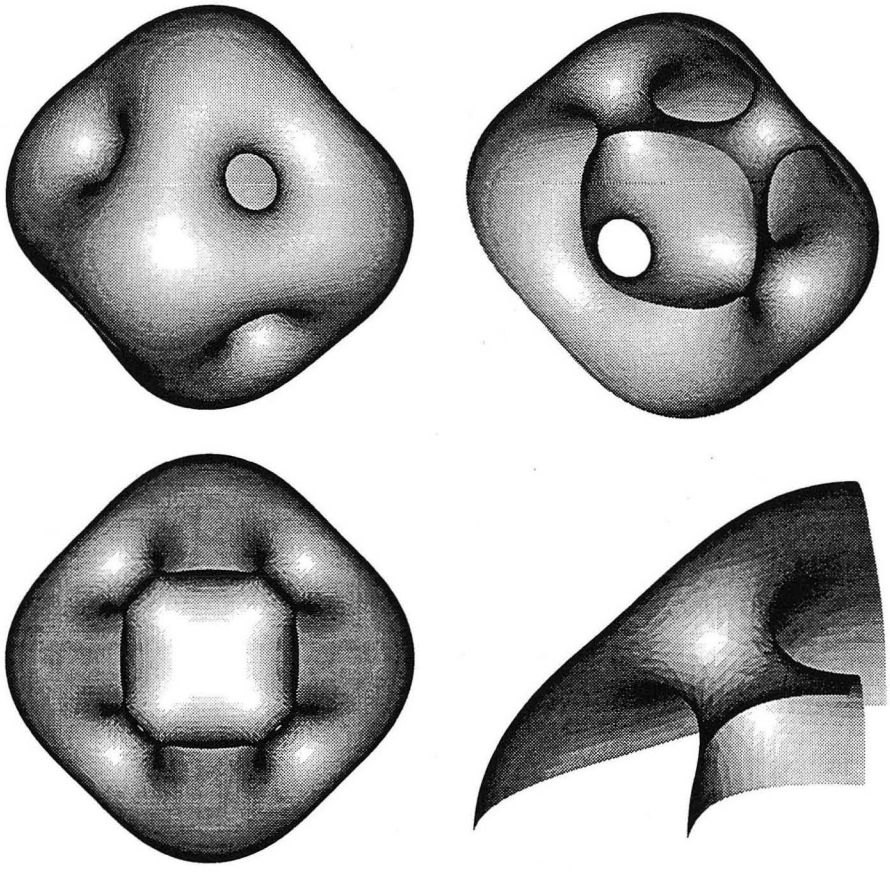

Figure 17: Self-similar octahedron surface

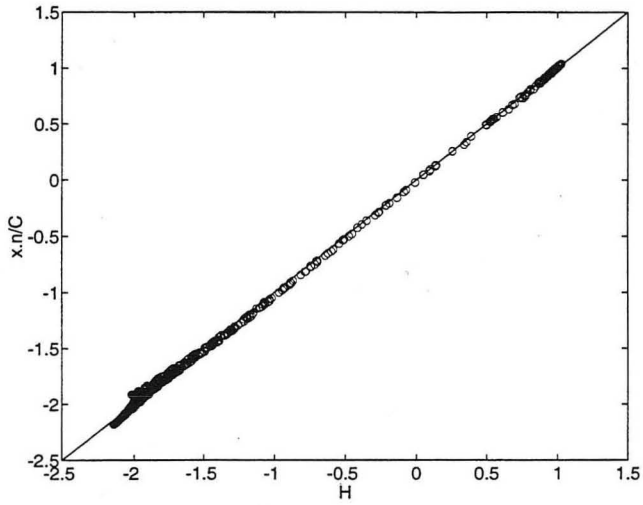

Figure 18: Graph of $\frac{1}{C}x_i \cdot n_i$ versus H_i for octahedron

remaining level sets were equidistant contours from the initial surface. For this surface, a ratio function was needed. It measured the cross-sectional area of the top handle over the cross-sectional area of the middle hole. The cross-sectional area of the top handle was also used for the volume computation similar to the previous example.

The final computed solution is shown in Figure 25. The computation was performed on a 100x100x100 grid with space step $\Delta x = 2.02 \times 10^{-2}$. The computed error for this surface is $E = 5.588 \times 10^{-2}$. The plot of $\frac{x_i \cdot n_i}{2T}$ versus H_i is shown in Figure 26. For purposes of computing the error, the points of

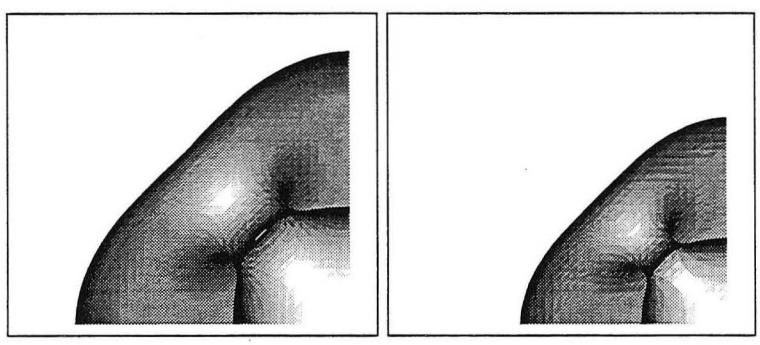

Figure 19: Octahedron evolved by mean curvature flow

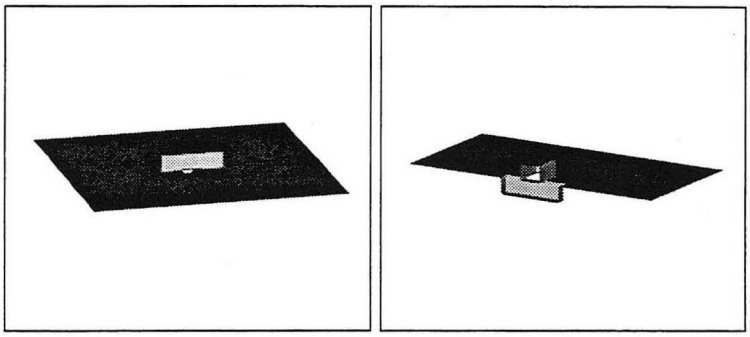

Figure 20: Initial surface for the "Punctured Saddle"

the surface on the boundary of the domain have been excluded. The tests for self-similarity indicate that this surface is also self-similar.

This example, if it can be proved to exist, may also be a candidate for an initial smooth surface which develops an interior. Asymptotically, the surface appears to be a cone so that at the time of singularity the surface should form an actual cone. A cone surface does form an interior according to the theory of weak solutions. This surface would then close a gap in the theory of mean curvature flow.

5 Conclusion and Future Work

We have presented here an algorithm which we believe is capable of computing self-similar solutions of mean curvature flow. In particular, we have computed self-similar surfaces which have been speculated to exist, but have not been verified theoretically. In particular, the "Double Handle" surface may contribute substantially to closing the gap in understanding mean curvature flow and the types of singularities that can occur from initially smooth surfaces. We hope that these solutions will also aid in proving the existence (or non-existence) of new self-similar solutions.

One shortcoming of this approach is the symmetry restriction for solutions. We intend to remove one degree of freedom from this restriction by increasing the dimension of the space $S_\lambda(0)$ to two, and thus the space U will have dimension three. In this case, we will have two ratio functions ρ_1, ρ_2 for selecting trajectories within U. The resulting calculation should be possible within R^4, otherwise the computing expense will be too great.

In this higher dimension, we hope to find more self-similar solutions which are not currently possible with the current method. Two of our intended solutions will be semi-regular polyhedra and a trefoil knot amongst others.

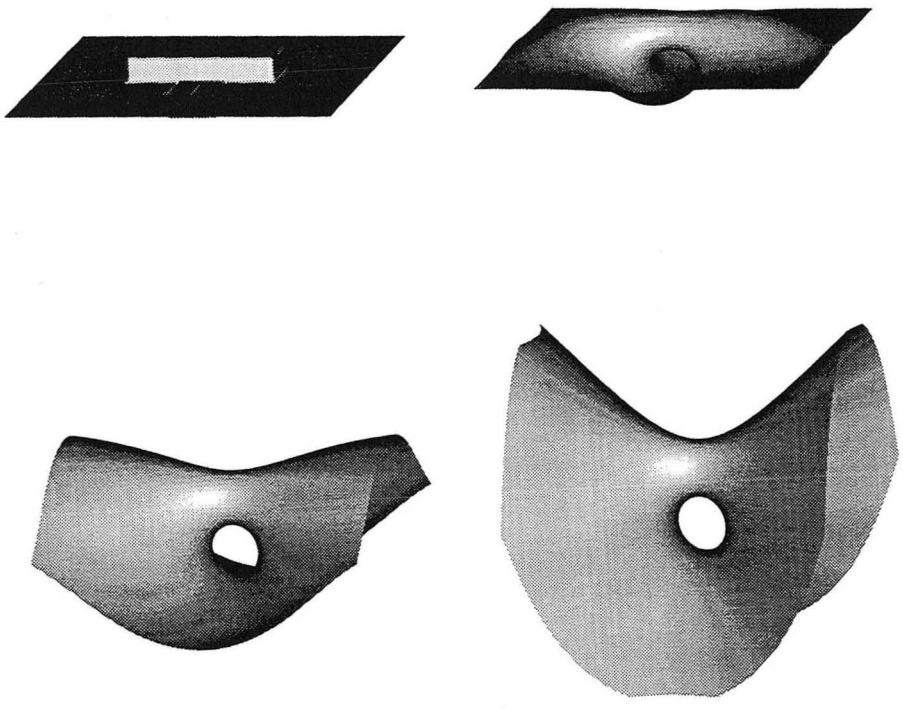

Figure 21: Evolution of the "Punctured Saddle"

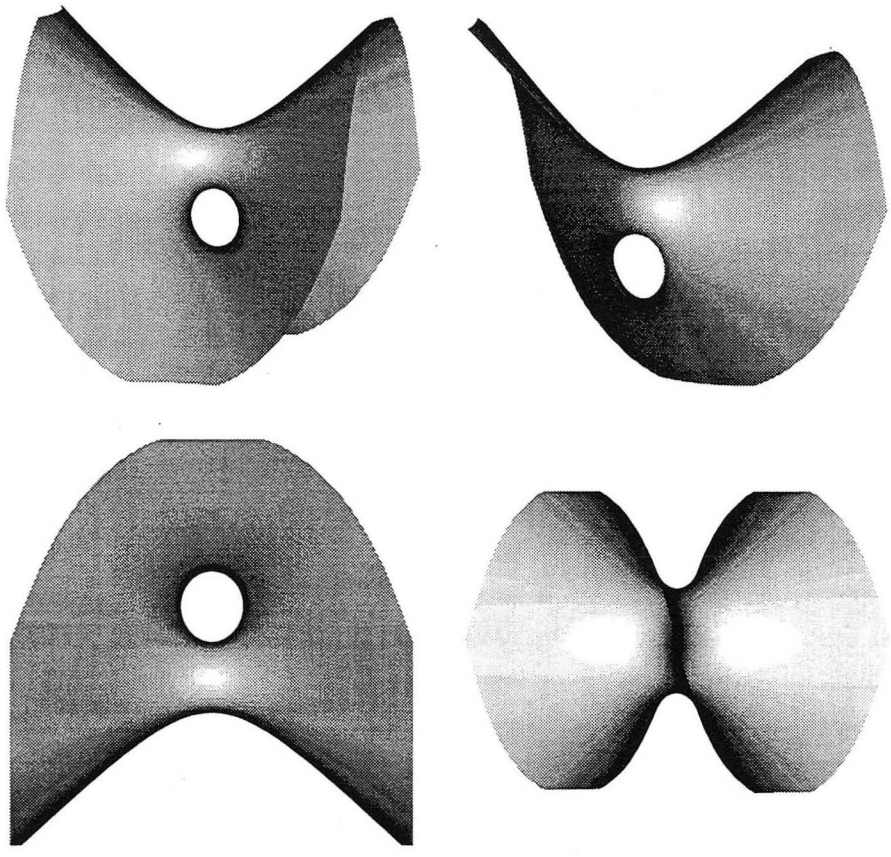

Figure 22: Pictures of the "Punctured Saddle" solution

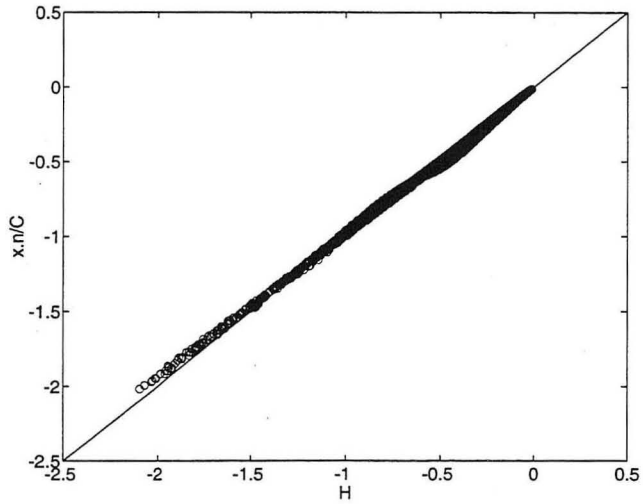

Figure 23: Graph of $\frac{1}{\bar{C}} x_i \cdot n_i$ versus H_i for the Punctured Saddle

5.1 Acknowledgments

We would like to thank L. Craig Evans, Tom Ilmanen, Doug Jungreis, James Sethian, Sigurd Angenent, Gerhard Huisken, Peter Smereka, and Stan Osher for helpful comments and suggestions. A video tape of these surfaces is available from the author upon request. We would like to thank Wes Bethel and the Graphics Group of the Information and Computing Sciences Division, Lawrence Berkeley Laboratory for their assistance in creating the video.

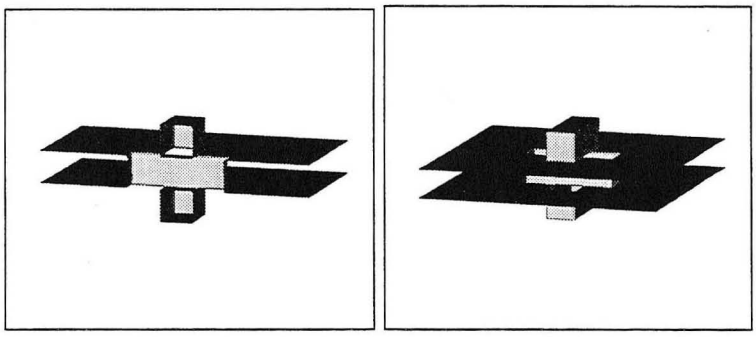

Figure 24: Initial surface for the "Double Handle"

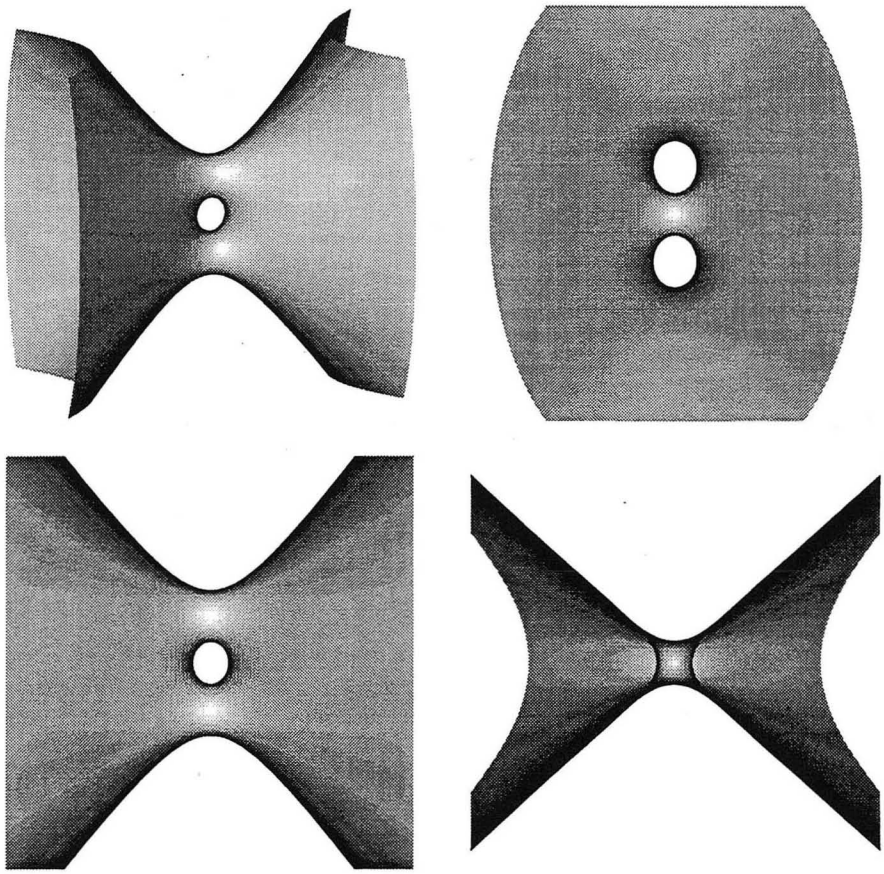

Figure 25: Pictures of the "Double Handle" solution

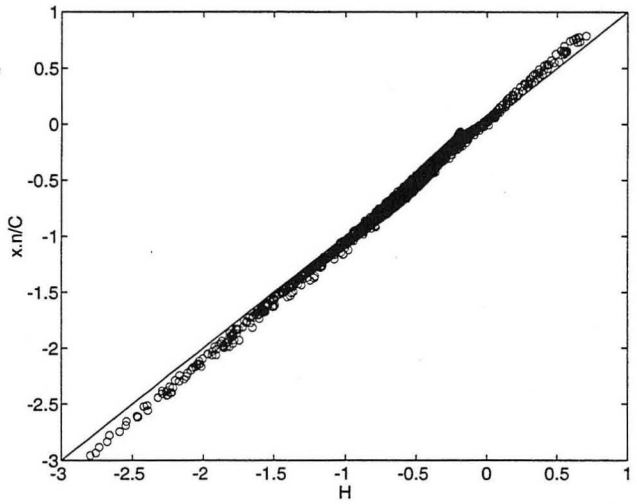

Figure 26: Graph of $\frac{1}{C}x_i \cdot n_i$ versus H_i for the Double Handle

References

[1] S. Altshuler, S. B. Angenent, and Y. Giga. Mean curvature flow through singularities for surfaces of rotation. preprint, 1993.

[2] S. Angenent. Shrinking doughnuts. In *Nonlinear Diffusion Equations and Their Equilibrium Stats, 3*, 1992.

[3] Y. Chen, Y. Giga, and S. Goto. Uniqueness and existence of viscosity solutions of generalized mean curvature flow equations. *Journal of Differential Geometry*, 33:749–786, 1991.

[4] D. L. Chopp. Flow under geodesic curvature. Technical Report CAM 92-23, UCLA, May 1992.

[5] D. L. Chopp. Computing minimal surfaces via level set curvature flow. *Journal of Computational Physics*, 106(1):77–91, May 1993.

[6] D. L. Chopp and J. A. Sethian. Flow under mean curvature: Singularity formation and minimal surfaces. Technical Report PAM-541, Center for Pure and Applied Mathematics, University of California, Berkeley, November 1991.

[7] L. C. Evans, H. M. Soner, and P. E. Souganidis. Phase transitions and generalized motion by mean curvature. *Communications on Pure and Applied Mathematics*, 45(9):1097–1123, 1992.

[8] L. C. Evans and J. Spruck. Motion of level sets by mean curvature I. *Journal of Differential Geometry*, 33:635–681, 1991.

[9] L. C. Evans and J. Spruck. Motion of level sets by mean curvature II. *Transactions of the American Mathematical Society*, 330:321–332, 1992.

[10] M. Falcone, T. Giorgi, and P. Loretti. Level sets of viscosity solutions and applications. Technical report, Instituto per le Applicazioni del Calcolo, Rome, 1990. preprint.

[11] Y. Giga and S. Goto. Motion of hypersurfaces and geometric equations. *Journal of the Mathematical Society of Japan*, 44(1):99–111, 1992.

[12] M. Grayson. The heat equation shrinks embedded plane curves to round points. *Journal of Differential Geometry*, 26(285), 1987.

[13] M. Grayson. A short note on the evolution of surfaces via mean curvature. *Duke Mathematical Journal*, 58:555–558, 1989.

[14] G. Huisken. Flow by mean curvature of convex surfaces into spheres. *Journal of Differential Geometry*, 20:237–266, 1984.

[15] G. Huisken. Asymptotic behavior for singularities of the mean curvature flow. *Journal of Differential Geometry*, 31:285–299, 1991.

[16] S. Osher and J. A. Sethian. Fronts propagating with curvature-dependent speed: Algorithms based on Hamilton-Jacobi formulations. *Journal of Computational Physics*, 79(1), November 1988.

[17] J. A. Sethian. Curvature and the evolution of fronts. *Communications in Mathematical Physics*, 101:487–499, 1985.

[18] J. A. Sethian. A review of recent numerical algorithms for hypersurfaces moving with curvature-dependent speed. *Journal of Differential Geometry*, 31:131–161, 1989.

[19] J. A. Sethian and J. Strain. Crystal growth and dendrite solidification. *Journal of Computational Physics*, 98(2):231–253, 1992.

LAWRENCE BERKELEY LABORATORY
UNIVERSITY OF CALIFORNIA
TECHNICAL INFORMATION DEPARTMENT
BERKELEY, CALIFORNIA 94720